Evolution of aerial spider webs coincided with repeated structural optimization of silk anchorages

EVOLUTION
INTERNATIONAL JOURNAL OF ORGANIC EVOLUTION
SSE
SOCIETY for the STUDY of EVOLUTION

Evolution of aerial spider webs coincided with repeated structural optimization of silk anchorages

Journal:	*Evolution*
Manuscript ID	19-0218
Manuscript Type:	Original Article
Keywords:	animal architecture, evolutionary biomechanics, extended phenotype, spider silk

Evolution of aerial spider webs coincided with repeated structural optimization of silk anchorages

Abstract

Physical structures built by animals challenge our understanding of biological processes and inspire the development of smart materials and green architecture. It is thus indispensable to understand the drivers, constraints and dynamics that lead to the emergence and modification of building behaviour. Here, we demonstrate that spider web diversification repeatedly followed strikingly similar evolutionary trajectories, guided by physical constraints. We found that the evolution of suspended webs that intercept flying prey coincided with small changes in silk anchoring behaviour with considerable effects on the robustness of web attachment. The use of nanofiber based capture threads (cribellate silk) conflicts with the behavioural enhancement of web attachment, and the repeated loss of this trait was frequently followed by physical improvements of web anchor structure. These findings suggest that the evolution of building behaviour may be constrained by major physical traits limiting its role in rapid adaptation to a changing environment.

Keywords

animal architecture; macro-evolution; evolutionary biomechanics; extended phenotype; spider silk; bio-inspiration

Introduction

From efficient tunnel networks of ant colonies and strikingly effective thermal control of termite mounds to the aesthetic assembly of bower bird displays and ecosystem-forming beaver dams: the complexity, efficiency and far reaching effects of animal buildings excite and inspire (Hansell 2005) - their study may even drive technical innovation towards a greener future (Turner and Soar 2008). Our understanding of how building behaviour evolves within an ecological context is limited because animal architectures blur the boundaries of an organism's phenotype (Dawkins 1982; Odling-Smee et al. 2003; Bailey 2012).

Spider webs are flagship examples of animal architectures, and their enormous diversity in shape render them an ideal system in which to unravel the evolutionary dynamics of building behaviour. Hypotheses of spider web evolution have been formulated for more than a hundred years, with a focus on the role of putatively singular events, such as the emergence of distinct building routines, specific silk proteins or viscid silk (Coddington 1986; Eberhard 1990; Bond and Opell 1998; Coddington 2005; Blackledge et al. 2009). In contrast, recent (Bond et al. 2014; Fernández et al. 2014; Fernández et al. 2018) and controversial (Garrison et al. 2016; Eberhard 2018a) phylogenomic studies favour a more dynamic scenario, where similar behavioural routines have repeatedly evolved. The core of the controversy is the question whether the evolution of behavioural building routines is dynamic and repeatable or slow and determined by contingent events. The answer to this question goes beyond spider webs: if the evolution of behaviour is less constrained than the evolution of physiological and morphological traits it could facilitate rapid responses to environmental changes, thereby setting the course of evolutionary trajectories (Wcislo 1989; Odling-Smee et al. 2003; Ord and Summers 2015).

Here, we approach the inference of spider web evolution from a previously neglected angle: the idea that a robust foundation is the basis for a stable building (Hansell 2005). It has been proposed that the evolution of tape-like thread anchorages at the base of modern spiders (Araneomorphae) ~300 MYA dramatically changed silk usage: spiders were no longer restricted to spinning substrate-bound sheets, but could produce complex three dimensional structures by spatially arranging single lines (Coddington 2005; Wolff et al. 2017). Despite this early insight, subsequent work has focussed on the role web geometry and silk proteins in the evolution of webs, neglecting the role of web anchorages.

Since anchor strength underlies global mechanical rules, it is possible to derive parameter estimates for its physical optimization (Pugno et al. 2013). A previous parametric study by two of us revealed that a single parameter in anchor structure (i.e. the location of the dragline joint) explains most of the variation in anchor strength (Wolff and Herberstein 2017).

We hypothesized that lineages that achieve optimal anchor strength by behavioural means, also achieve web types with greater mechanical integrity. To test this, we quantified silk anchor structure and web types in 105 spider species of 45 families, covering all major clades of the modern spiders. We first built a numerical model to identify the optimum in anchor structure and tested if it matched the adaptive peaks in the macro-evolutionary signal. We then related silk anchor performance to anchor building behaviour and the morphology of the spinning apparatus. Specifically, we tested how the innate spinneret choreography during anchor production affects anchor structure (Wolff et al. 2017), and how the configuration of the spinning apparatus affects the kinematic properties of the system. Here we distinguished between such spiders that bear a spinning plate, the so-called *cribellum*, in the anterior part of the spinning apparatus (cribellate spiders) and such, in which this organ is reduced and non-functional (ecribellate spiders). The cribellum is used to produce sophisticated adhesive capture threads, representing bundles of nano-fibres, and we hypothesized that it restricts the mobility of the spinnerets involved in silk anchor production. Finally, we aimed to determine the sequence of silk anchor enhancement and aerial web evolution: did an evolutionary enhancement of silk anchors occur after the evolution of aerial webs, or did enhanced anchors precede the evolution of aerial webs? Such time sequences could provide insights into whether silk anchor mechanics constrain or facilitate the evolution of web architectures.

Material and Methods

Material sourcing and fieldwork

Spiders were collected in Eastern Australia (NSW, QLD, VIC and TAS), New Zealand (North Island), Germany, Italy, the U.S.A., Argentina and Morocco, or obtained from lab stocks (3 species) and kept in the lab in plastic jars or boxes with slightly moistened tissue (complete list of species and collection data in Tab. S9). We aimed for three individuals per species, while we did not expect differences in our target traits between sexes and developmental stages (confirmed by intraspecific comparison of anchor structure in *Argiope keyserlingi* and *Nephila plumipes*, unpub.). However, for some species only single individuals could be obtained (samples sizes are given in Tab. S9 and Fig. 2). Silk samples were collected on glass slides that were left in the enclosures for 2-7 days. Silk samples were stored in dry boxes and are deposited at the Department of Biological Sciences, Macquarie University (MQ). Voucher specimens of spiders are deposited at the Australian Museum (AM), the Zoological Museum of the University of Greifswald (UG), the Natural History Museum of Argentina (MA), Canterbury Museum (CM) and private collections (see Tab. S9 for details).

For each species we recorded the web type based on field and lab observations: 0, no web (hunting spider); 1, substrate bound web (capture area ± parallel and directly attached to the substrate surface); 2, aerial web (capture area suspended, indirectly attached to substrate, and its shape ± independent of substrate topography). These categories were chosen, because they represent different demands of a robust anchorage.

Morphology of spinning apparatus

Spiders were investigated under dissection microscopes to score two states of the spinning apparatus: 0, ecribellate; 1, cribellate.

Kinematics of spinning apparatus

Spinning choreography was studied in a subset of 71 species following the methods described in (Wolff and Herberstein 2017), using a Basler Ace 640×480pix USB 3.0 high speed video camera (Basler AG, Ahrensburg, Germany), equipped with a Navitar Precise Eye extension tube including a 1.33× magnification lens (Navitar, Inc., Rochester, NY, USA). A 0.25× accessory lens was used for larger spiders (body length >10 mm). The resulting field of view was 1.3 × 1.0 mm at a pixel size of 2.1 µm for the basic configuration, and 5.3 × 4.0 mm at a pixel size of 8.3 µm for the configuration with the 0.25× lens. Videos were recorded with 500 frames per second, using the *TroublePix* software (NorPix, Inc., Montreal, QC, Canada) with continuous looping and post event trigger.

Videos were processed with *ImageJ 1.5* (Schneider et al. 2012) as detailed in (Wolff and Herberstein 2017). The movements of both anterior lateral spinnerets were manually tracked using the *MTrackJ* plugin (Meijering et al. 2012), taking the centre of the piriform spigot field on the anterior lateral spinneret apex as a reference. Each spinning sequence consists of a set of stereotypic spinneret trajectories. Single trajectories were extracted, their tracking coordinates positioned in a generalized grid and partitioned into 50 landmarks defined by regularly spaced time intervals (for details on this procedure we refer to (Wolff and Herberstein 2017; Wolff et al. 2017)). This procedure ensures that the relative orientation of the kinematic track shapes towards the animal's body axis is maintained. From these shapes we calculated the relative track proportions h_r as the y-dimension divided by the x-dimension of the aligned track shape, where the minimal x-coordinate denotes the proximal turning point of the adducted spinneret (where the dragline is usually placed) and the maximal x-coordinate the lateral turning point of the abducted spinneret. This variable reflects under which angle piriform silk is spread away from the dragline joint.

The final dragline location may not only be determined by the trajectories of single kinematic elements, but also how these are applied along the animal's body axis. Some spiders perform a back-and-forth movement of the abdomen to further modulate dragline placement. This behaviour was recorded as a binary character: 0, absent; 1, present.

Structure and morphometrics of silk anchors

Nine to twenty silk anchors per individual spider were imaged with Leica M205A (Leica Microsystems GmbH, Wetzlar, Germany) and Motic (Motic Inc. Ltd., Hong Kong) stereo microscopes with mounted cameras.

Morphometrics of silk anchors was performed on micrographs in *ImageJ*. We calculated the dragline placement variable c_d as follows: distance d between the dragline joint (point were the dragline leaves the anchor) and the anterior border of the anchor divided by the longitudinal dimension of the anchor. In anchors of some basal species the individual dragline fibres do not leave the anchor as a bundle, but separately in different locations. In these cases the pair of fibres located closest to the frontal border of the anchor was taken into consideration and their d-values were averaged. Details on the morphometric characterization of silk anchors are described in (Wolff and Herberstein 2017).

Numerical model

The elastic membrane was modelled by discretising it in a network of elastic bonds (i.e. springs) in a square-diagonal lattice, using a generalized non-linear 3D co-rotational truss formulation (Cook et al. 2001). A homogenization procedure was adopted, imposing the equivalence of the strain energy density of the lattice with that of a corresponding homogeneous membrane (Ostoja-Starzewski 2002; Brely et al. 2015). We used a standardized anchor geometry with length l = 1 mm, width w = 1 mm, thickness t = 1 µm, and with the dragline fused with the membrane over a length of c_l = 0.33 mm. To account for differences in silk properties, we performed separate simulations for a combination of membrane and dragline stiffness values, as empirically observed in the basal sheet web spider *H. troglodytes* and the aerial web builder *N. plumipes*: Young's modulus of piriform silk membrane E_p = 0.25 GPa for *Hickmania* and E_p = 1.7 GPa for *Nephila* (see tensile test methodologies and results in S1), and Young's modulus of dragline E_d = 10 GPa for *Hickmania* and E_d = 15 GPa for *Nephila* (after (Piorkowski et al. 2018) and (Swanson et al. 2006)).

The interface was modelled assuming a 3D exponential-like traction-separation law (cohesive zone model) of the form $T_i = \Delta_i \frac{\phi_i}{\delta_i^2} \cdot \exp\left(\sum_j - \frac{\Delta_j^2}{\delta_j^2}\right)$ where ϕ_i, Δ_i and δ_i are the work of

159 separation, the crack gap value and the characteristic length (i.e. the gap value corresponding
160 to the maximum traction) (Salehani and Irani 2018). The resulting system of coupled non-linear
161 equations in matrix form was solved using an algorithm based on the Newton-Raphson method
162 (Ostrowski 1973) implemented in C++ and run on the OCCAM HPC cluster at the University
163 of Torino. The adhesive energy of the interface, calculated as the integral of the cohesive law,
164 was taken to be equal to $\phi = 0.5$ MPa·mm.

165 We simulated the maximal pull-off forces for different c_d between 0.0 and 0.5. To
166 further study the effect of c_d on anchor robustness we simulated maximal pull-off forces for
167 different pull-off angles (loading angles) between 15° (± parallel to substrate along spinning
168 direction) and 165° (± parallel to substrate against spinning direction, e.g. dragline flipped over)
169 for a c_d of 0.0, 0.2 and 0.4.
170
171 *Phylogenetic inference*
172 The phylogenetic tree was estimated using three mitochondrial (12S, 16S, COI) and
173 three nuclear (histone H3, 18S, 28S) markers, taken from the study of Wheeler et al. (2017) and
174 supplemented with sequences from GenBank (Tab. S11). The clades obtained as monophyletic
175 in the genomic analyses of Fernández et al. (2018) (Araneae), Kallal et al. (2018) (Araneidae),
176 Cheng and Piel (2018) (oval calamistrum clade), and Maddison et al. (2017) (Salticidae) were
177 constrained for monophyly, as a backbone tree. The reason for such constrained analysis is that
178 our six-markers dataset will not have sufficient signal to overturn the results based on hundreds
179 to thousands of markers from the genomic analyses.
180 We lacked sequence data for 58 of the studied species but were able to use sequences
181 from closely related species to obtain a good estimate of phylogenetic placement and branch
182 lengths (Tab. S10). For an additional set of 20 species we did not have close relatives, or a close
183 relative was already in the dataset; these were connected randomly in internal branches
184 according to their taxonomic placement (Tab. S10). Two non-araneomorph terminals were
185 added to root the tree, representing the lineages Mesothelae and Mygalomorphae; these were
186 excluded from the comparative analyses.
187 Alignment of sequences was performed with *MAFFT* version 7 online service (Katoh et
188 al. 2017). Model selection was made with *jModeltest* (Darriba et al. 2012). Secondary dating of
189 main tree nodes was assigned as mean and 95% HPD taken from Fernández et al. (2018) and
190 analysed in *BEAST2* (Bouckaert et al. 2014) under a relaxed lognormal clock model
191 (Drummond et al. 2006), using the CIPRES Science Gateway (Miller et al. 2010) for 50 million
192 generations. After a pilot run, GTR models were simplified to HYK to achieve convergence.

The 20 species without sequence data were free to connect anywhere along any branch within taxonomically constrained clades; to avoid for very short tip branches, we placed a uniform prior for the clade age, with minimum 2 mya for congeners and 5 mya for higher taxa.

To account for the uncertainty of the phylogenetic estimation, we obtained 100 trees randomly drawn from the post-burnin posterior sample of the Bayesian analysis in *BEAST2*. The subsequent comparative analyses are averaged over these 100 trees, and thus incorporate the uncertainty in phylogenetic parameters.

Macro-evolutionary framework

We used phylogenetic comparative methods to infer adaptive peaks and constraints and test evolutionary associations of silk anchor structure, spinning apparatus, spinning kinematics and web building behaviour, using multiple packages in the software environment *R*.

To select the best model for ancestral character estimation (*ACE*), we calculated the corrected Akaike information criterion weights (*AICcw*) using *geiger* 2.0.6 (Pennell et al. 2014). For spinning apparatus state, we fitted an Equal Rates model (*ER*), an All Rates Different model (*ARD*) and a customized model with supressed state 1 to 2 transitions (following Dollo's law, see (Alfaro et al. 2018)), of which the Dollo's law model had the strongest support (*AICcw* = 0.640). For web type ER, SYM and ARD models were fitted, of which the ER model was preferred (*AICcw* = 0.583). ACE was performed with stochastic character mapping in *phytools* (Revell 2012), on the consensus tree with 100 repeats and across a sample of 100 trees with 1 simmap per tree.

To infer evolutionary dynamics of the continuous variables dragline placement c_d and spinning track dimensions h_r we used a multi-step model-selection process. To test if changes in discreet characters led to differential evolutionary dynamics, we fitted different Brownian Motion (*BM*) and generalized Ornstein-Uhlenbeck-based Hansen models (*OU*) using the package *OUwie* 1.50 (Beaulieu and O'Meara 2014). We built a set of models for spinning apparatus state (*c*) and web type (*w*, web type was binary discretized for this purpose in aerial web: 0, no; 1, yes) using a randomly drawn simmap of *c*- and *w*-regimes for each of the 100 trees from our sample. We tested a single-regime BM (*BM1*) and OU model (*OU1*), and per regime type each a two-σ^2 (*BMS*) BM model, and OU models with two θ (*OUM*), two θ and two σ^2 (*OUMV*), two θ and two α (*OUMA*), and two θ, two σ^2 and two σ^2 (*OUMVA*). The *AICcw* was used to compare the fit between all 12 models for each tree. *AICcw* and model parameters were then summarized across all 100 trees and their median and variance assessed to select for the model(s) that could best explain the data. For each c_d and h_r we ran two loops across the

tree sample to check for the effect of the stochastic component in this procedure, and found comparable results (i.e. similar models were favoured and no major differences in median parameter estimates).

While prior clade assignments are useful to compare defined groups, they may miss some hidden patterns caused by unstudied effects. We therefore additionally used the methods *SURFACE* (Ingram and Mahler 2013) and *bayou* (Uyeda and Harmon 2014) on the consensus tree (S3). *SURFACE* performs stepwise AIC estimation to identify regime shifts in θ assuming evolution under the OU process with constant σ^2 and α. *bayou* uses a reverse-jump Markov chain Monte Carlo procedure for the similar purpose. By this, we also checked, if evolution of our variables was driven by singular events (i.e. the occurrence of only a single shift), which may bias PGLS inference (Uyeda et al. 2018). Priors in *bayou* analyses were defined as follows: for α a half-Cauchy distribution with *scale* = 0.1; for σ^2 a half-Cauchy distribution with *scale* = 0.01; for θ a uniform distribution delimited by *min* = 0 and *max* = 1; and a conditional Poisson for the number of shifts. Because the results of *bayou* can be sensitive to the mean number of shifts in the prior (Ho and Ané 2014; Uyeda and Harmon 2014), we ran each two chains over 500,000 generations for prior means of 10, 15, 20, and 25 shifts with equal shift probability and one shift maximum per branch, discarding the first 30% as burn-in. For c_d chains with priors of 20 and 25 shifts and for h_r chains with priors of 15, 20 and 25 shifts arrived at a similar posterior (S6). Results are reported from these chains only (means of converged chains given, and graphical representation of shifts for c_d from a randomly chosen chain with a prior of 25 shifts and for h_r from a randomly chosen chain with a prior of 20 shifts).

Trait correlation

To reveal patterns of trait correlation we used phylogenetic generalized least squares models (PGLS), which accounts for the non-independence of observations due to common evolutionary history (Felsenstein 1985; Grafen 1989; Freckleton et al. 2002), across pairwise combinations of our variables: (1) $c_d \sim$ *spinning apparatus*; (2) $c_d \sim$ *web type*; (3) $h_r \sim$ *spinning apparatus*; and (4) $h_r \sim$ *web type*. Further, we performed PGLS regressions between $c_d \sim h_r$. PGLS analyses were performed with the R package *phylolm* (Tung Ho and Ané 2014) and branch length transformation were optimized by setting *lambda* value through maximum likelihood. To account for phylogenetic uncertainty in PGLS results (Donoghue and Ackerly 1996) we repeated each model across our posterior sample of 100 phylogenetic trees. The influence of phylogenetic uncertainty on results was estimated by the variation in model

parameters across all runs. Phylogenetic sensitivity analyses were performed for each PGLS model with the R package *sensiPhy* (Paterno et al. 2018).

Geometric Morphometrics

To test if the shape of spinning paths differed between spiders with different spinning apparatus and web type, and if it correlates with c_d and h_r, geometric morphometrics was performed using the R package *geomorph* (Adams and Otárola-Castillo 2013). For this purpose aligned spinneret trajectories were discretized into 50 landmarks with similar time steps, as described in (Wolff et al. 2017). We used both an alignment towards the median axis between the paired spinnerets which keeps the angular orientation of the trajectories (see (Wolff et al. 2017)), and General Procrustes Alignment (GPA), which omits this information and extracts the pure shape. We then performed Phylogenetic Procrustes ANOVA against the variable 'spinning apparatus' and 'web type' and Phylogenetic Procrustes Regression against variables c_d and h_r using the consensus tree.

Results

Physical constraints and optima of silk anchorages

Our broad comparative study of anchor structures across the spider tree of life confirmed that there is a general structure of web anchors, consisting of a dragline attached to the substrate with numerous, sub-micron sized, glue coated fibres (*piriform silk*) combined into a patch-like film. The major interspecific differences are the shape of the piriform silk film and the structure of the dragline joint. The dragline can be embedded all the way through this film, or be attached centrally only. The attachment position of the dragline greatly affects where and how load is transmitted onto the underlying film. The more central the dragline placement c_d (i.e. the dragline centrality) the better the anchor can withstand stress from a variably loaded silk line. Preliminary studies have revealed that this is the most significant determinant of web anchor robustness (Wolff and Herberstein 2017).

To identify the optimum of the dragline placement parameter, we built a numerical model based on the theory of thin film contact mechanics (Pugno 2011), approximating silk anchorages as tape like films. Previous models of web anchor mechanics, such as the staple-pin model (Sahni et al. 2012; Pugno et al. 2013), do not account for the observed variation in dragline joint structure and presume independent peeling events of single piriform fibres, which, however, have not been empirically observed in peel-off tests with attachment discs from orb web spiders (Araneidae) and wandering spiders (Ctenidae) (Wolff et al. 2015; Wolff

294 2017; Wolff and Herberstein 2017). In our comparative analysis reported here, we did not
295 observe a single case of an attachment disc composed of parallel piriform fibres that did not
296 overlap with each other, confirming that the staple-pin model is not appropriate to describe the
297 mechanics of spider web anchorages. We therefore developed a new model, approximating the
298 piriform silk film as a single tape-like element, where load is shared and transmitted between
299 piriform fibres.
300 To apply our results to a range of silk properties found in spiders, we repeated
301 simulations for parameters measured in the Tasmanian cave spider (*Hickmania troglodytes*),
302 representing an ancient lineage, and in golden orb web spiders (*Nephila plumipes*), a
303 representative of derived aerial web builders. We found that anchor strength improved if its
304 geometrical structure is allowed to maximize the peeling line (total length of the detachment
305 front) before detachment, which occurred in the range c_d = 0.3–0.5 mm/mm for typical
306 anchorage parameters (Fig. 1a). The exact optimum within this range depends, amongst others,
307 on the material properties of the silk. For draglines as stiff as the anchor silk (or point-like
308 dragline joints) c_d = 0.5 and it decreased with an increase in stiffness difference between
309 dragline and anchor silk. During detachment, the stress concentrations and subsequent
310 delamination front approximated a circular shape that became more elliptical as the peeling
311 angle increased (Fig. 1b). The c_d value determined a delay in the detachment front reaching the
312 anchorage edges (for typical anchorage shapes), leading to an overall increase in robustness.
313 This is in agreement with empirical data on silk anchors of orb web spiders (S2) and up-scaled
314 physical models (Wolff and Herberstein 2017). Notably, the effect of the pulling angle on
315 anchor resistance was reduced at optimal c_d (Fig. 1c,d). This indicates that the benefit of high
316 c_d is realised in dynamic loading situation, such as in aerial webs.
317
318 *Evolutionary dynamics of spider web traits*
319 Spider webs are diverse in shape and function but for the purpose of our analyses we
320 categorised the web phenotypes into: ‘substrate webs’, ‘aerial webs’ and ‘webless foragers’
321 (see methods for definition). Aerial webs were hereby characterized by a capture area (sheet or
322 tangle) that is fully suspended (i.e. indirectly attached to the substrate by supporting lines) and
323 has a shape that does not resemble the substrate topography, such as in orb webs, cob webs and
324 canopy webs. This categorization followed the assumption that such aerial webs often have an
325 increased demand in anchor robustness, because of the use of a limited number of anchor lines
326 and higher exposure to mechanical impacts, such as wind, rain and flying animals. Our
327 phylogenetic analyses indicated that substrate webs are the ancestral state in the

Araneomorphae and aerial webs have evolved five to six times independently: at the basis of Araneoidea, in Uloboridae, Deinopidae, Pholcidae, and within Desidae (Fig. 2; S4).

We found, that lineages with anchors near the physical optimum of c_d = 0.3–0.5 included all aerial web builders that lack a cribellum, one cribellate substrate web building species (*Megadictyna thilenii*), and some ecribellate hunting spiders belonging to Mimetidae, Arkyidae, Thomisidae, Oxyopidae, Trechaleidae, Philodromidae, Salticidae and Toxopidae. We found multiple support for six shifts in the evolutionary regime of c_d (Fig. 2; S5): *shift 1* in Pholcidae (posterior probability *pp* = 0.494); *shift 2* in the grate-shaped tapetum clade (excl. Zoropsidae) (*pp* = 0.474); *shift 3* at the basis of Salticidae (*pp* = 0.405); *shift 4* at the basis of Entelegynae (*pp* = 370); *shift 5* at the basis of Araneoidea (*pp* = 0.336); and *shift 6* within Desidae (*Cambridgea*) (*pp* = 0.309). Shift 5 and 6 (both aerial web spinners; adaptive optimum $\theta \sim 0.36$ mm/mm), and shifts 1, 2 and 3 (aerial web spinning and hunting spiders; $\theta \sim 0.30$ mm/mm) were convergent, shifting towards similar evolutionary optima (Fig. 3f). Shifts 2, 5 and 6 coincided with cribellum loss and shifts 1 and 5 with the evolution of aerial webs. Notably all supported shifts led towards an elevated adaptive optimum θ. Our data suggest that the evolutionary trend towards an elevated c_d happened stepwise, for instance the exceptional c_d in Araneoidea evolved from an estimated root optimum of $\theta \sim 0.18$ mm/mm, with the first shift around 250 MYA towards $\theta \sim 0.24$ mm/mm, and the second one around 180 MYA towards $\theta \sim 0.36$ mm/mm. The exact location of these shifts differed between *SURFACE* and *bayou* methods, and an additional shift at the basis of Nicodamidoidea+Araneoidea around 200 MYA is possible (Fig. 2; S5; S6).

We found strong correlations between c_d and the configuration of the spinning apparatus. Spiders with a cribellum (the basal state) produced a significantly smaller c_d (p = 0.005; S7) and cribellum loss repeatedly led to an increase of c_d (Fig. 2). Furthermore, c_d correlated with spinning choreography, i.e. the relative height of the spinneret trajectory geometry h_r (p = 0.004; S7): h_r is on average 1.6 times larger in ecribellate spiders ($p < 0.001$; S7). These results were highly robust to phylogenetic uncertainty (S7). Notably, the shape of the spinning path did not differ between cribellate and ecribellate spiders (p_r = 0.316) (S8). This indicates that it is not the shape of the spinning path, but its orientation and proportions that affect c_d. Our kinematic and morphological studies revealed that the cribellum mechanically constrains the mobility of the anchor producing spinnerets (the anterior lateral spinnerets) by blocking them on the anterior side. As a result, most cribellate spiders spread the spinnerets more laterally, leading to smaller h_r and c_d.

To further investigate if the configuration of the spinning apparatus (*c*) and web building behaviour (*w*) had an effect on the evolutionary dynamics of c_d, we compared the fit of single and two-regime Brownian Motion (BM) and Ornstein-Uhlenbeck (OU) models. To account for phylogenetic uncertainty, we repeated the analyses across a sample of 100 phylogenetic trees.

We found strong support for a scenario, where the evolution of anchor structure was highly dynamic in substrate web builders and hunters, but stabilized around an elevated optimum in aerial web builders. Among all models, OUw models provided the best explanation for the extant variation of c_d (*AICcw* (OUMVAw) = 0.667±0.339; *AICcw* (OUMAw) = 0.163±0.295; Fig. 3a). Under these models c_d evolved at an increased adaptive optimum with a high adaptive potential in aerial web builders, while c_d of substrate web building and hunting spiders followed a stochastic evolution (i.e. $t½ >> T$; Fig. 3b,c). There was support that cribellum loss affected the evolution of c_d (mean *ΔAICc* (OUMc-BM1) = 3.43, mean *ΔAICc* (OUMc-OU1) = 4.34). The best fit among OUc-models was the OUMc, a model under which c_d of ecribellate spiders had a higher adaptive optimum θ but evolutionary rates σ^2 and adaptive potential α did not differ between cribellate and ecribellate spiders. The inferred mean $t½$ was close to the total height of the tree *T*, which represents a moderate α (Cooper et al. 2016).

Similar analyses on the spinning track proportions h_r indicated five shifts in the evolutionary regime (Fig. 2; S5). All but one shift coincided with cribellum loss, and three shifts co-occurred with aerial webs. Branches accommodating shifts 1, 3, 4 and 5 also had shifts in c_d, indicating a causal link. The constitution of the spinning apparatus had clearly affected the evolution of h_r (*AICcw*(OUMAc) = 0.442 ±0.247; *AICcw*(OUMVAc) = 0.388 ±0.269), whereas OUw models were indistinguishable from BM models (Fig. 3d). The contrasting results for c_d indicate that h_r alone does not explain c_d. There is, at least, one additional behavioural component affecting c_d, which is the movement of the body while a series of alternating spinneret movements are performed. The highest c_d values (excluding the hunting spider *Australomisidia*) were found in spiders that perform a back-and-forth movement of the abdomen during anchor production. This behaviour has evolved independently in the Araneoidea and within the New Zealand Desidae.

Discussion

This study is the first to assess attachment as a component in the evolution of animal architectures. We have shown that small changes in anchor structure profoundly affect web attachment. Notably, structural optimization does not necessarily come at a higher material cost, as the effect of dragline placement is significant for similar sized silk films. It therefore appears

counter-intuitive that not all extant spiders exhibit an optimized anchor structure and that anchor building behaviour evolved slowly and stepwise. Our results indicate this is due to two reasons.

First, the evolution of anchor structure is relaxed in substrate web builders and wandering spiders. Substrate web builder rely less on robust silk anchorages, because their webs are attached with numerous anchor lines and are usually less exposed to the environment than aerial webs. Hunting spiders may have different demands on silk anchorages, depending on whether draglines are used for locomotion, or whether silk is merely used in substrate-bound sheets for shelters and eggs sacs. This may explain the high variation and lability of c_d in hunting spiders.

Second, the evolution of anchor building behaviour may be constrained by physical traits. Our data suggest that the cribellum organ, a sophisticated spinning plate that produces nanofiber-based capture threads, is one example of such a physical constraint on behavioural evolution. This is important since it provides an explanation for an old enigmatic problem in the understanding of spider web evolution: why nano-fibre capture silk was lost so frequently across the spider tree, resulting in cribellate spiders being largely outnumbered by ecribellate spiders, and why only few cribellate spiders evolved aerial webs, even though cribellate silk can be highly efficient in prey capture (Opell 1994; Opell and Schwend 2009; Bott et al. 2017). Our results indicate that the cribellum represents a significant physical constraint on the spinning of robust anchorages limiting the capability to build efficient suspended webs.

We found that all changes in the evolutionary mode of anchor spinning behaviour followed or coincided with the loss of the cribellum. However, not all events of cribellum loss were followed by changes in the evolutionary dynamics of spinning behaviour, indicating that further changes of physical traits, such as the arrangement of muscles and spinneret articulation, might have been necessary to alter spinning behaviour in a way to optimize anchor structure. Cribellum loss may thus rather be an important pre-condition for further evolutionary enhancement of silk attachment.

Multiple support for an exceptional (i.e. faster and more stabilized) evolution of anchor structure in aerial web builders suggests its adaptive value for such webs. Aerial webs repeatedly evolved after or with evolutionary shifts in silk anchor structure and anchor spinning behaviour occurred, supporting the idea that web anchor performance affects the evolution of web architecture.

Limited anchor performance may thus in itself be an important constraint in the evolution of web building behaviour, and its improvement may have accelerated spider web diversification: web architecture is phylogenetically labile and enormously variable in

ecribellate orb-web and cobweb spiders (Blackledge and Gillespie 2004; Eberhard et al. 2008; Kuntner et al. 2010), lineages in which anchor structure has reached the physical optimum. Such a rapid turnover of web building behaviour may mask evolutionary histories in these lineages. Concluding that similarities in building routines indicate a common origin can be problematic in these cases, since the probability of parallelism is high (Ord and Summers 2015; York and Fernald 2017). Nevertheless, we note that the idea of an independent origin of orb webs in Araneoidea and Uloboridae as indicated by this and a previous study (Fernández et al. 2018), has recently received some scepticism (Garrison et al. 2016; Coddington et al. 2018; Eberhard 2018b). In particular, it was argued that the loss of complex traits such as orb web building is more likely than their emergence, and the phylogenetic framework should account for that. Here, we tested three different evolutionary models, of which the *Equal Rates* model was statistically preferred. However, because our category 'aerial web' contains different architectural shapes of webs, our results are not suited to draw definitive conclusions on the homology of a single architectural type, such as orbs – a question that is outside the scope of this study. If assuming an early origin of the orb web at the root of Entelegynae, an early shift in the macro-evolutionary optimum of silk anchor structure (shift 4) would have coincided with the evolution of this ancient (cribellar) orb web. Thus, we refrain from drawing conclusions on the chronological order of web and web anchor evolution. Reconstructing the evolution of biomechanics and building routines of web elements other than anchors could help to resolve the chronology of evolutionary events that have preceded complex web architectures.

To the best of our knowledge, this is the first study that integrates physical and macro-evolutionary modelling to explain the evolution of animal architectures. Using web anchorages as an example, we demonstrate that to understand the evolution of complex behaviour, like web building, it is essential to identify the interdependencies of behavioural and physical traits. Future works should therefore study the evolution of animal architectures and the morphology of their architects in combination.

We conclude that the evolution of behaviour and extended phenotypes may be not as free as previously suggested (West-Eberhard 1989; Odling-Smee et al. 2003; Duckworth 2009; Bailey et al. 2018), but may rather be tightly bound to evolutionary changes in physical traits. In the case of spider webs the evolutionary removal of such physical constraints may have led to an evolutionary cascade resulting in an enormous diversity of web architectures and outstanding ecological success.

References

Adams, D. C. and E. Otárola-Castillo. 2013. geomorph: an R package for the collection and analysis of geometric morphometric shape data. Methods in Ecology and Evolution 4:393-399.

Alfaro, R. E., C. E. Griswold, and K. B. Miller. 2018. Comparative spigot ontogeny across the spider tree of life. PeerJ 6:e4233.

Bailey, N. W. 2012. Evolutionary models of extended phenotypes. Trends Ecol Evol 27:561-569.

Bailey, N. W., L. Marie-Orleach, and A. J. Moore. 2018. Indirect genetic effects in behavioral ecology: does behavior play a special role in evolution? Behav Ecol 29:1-11.

Beaulieu, J. and B. O'Meara. 2014. OUwie: analysis of evolutionary rates in an OU framework. R package version 1.

Blackledge, T. A. and R. G. Gillespie. 2004. Convergent evolution of behavior in an adaptive radiation of Hawaiian web-building spiders. Proceedings of the National Academy of Sciences 101:16228-16233.

Blackledge, T. A., N. Scharff, J. A. Coddington, T. Szüts, J. W. Wenzel, C. Y. Hayashi, and I. Agnarsson. 2009. Reconstructing web evolution and spider diversification in the molecular era. Proceedings of the National Academy of Sciences 106:5229-5234.

Bond, J. E., N. L. Garrison, C. A. Hamilton, R. L. Godwin, M. Hedin, and I. Agnarsson. 2014. Phylogenomics resolves a spider backbone phylogeny and rejects a prevailing paradigm for orb web evolution. Curr Biol 24:1765-1771.

Bond, J. E. and B. D. Opell. 1998. Testing adaptive radiation and key innovation hypotheses in spiders. Evolution 52:403-414.

Bott, R. A., W. Baumgartner, P. Bräunig, F. Menzel, and A.-C. Joel. 2017. Adhesion enhancement of cribellate capture threads by epicuticular waxes of the insect prey sheds new light on spider web evolution. Proc. R. Soc. B 284:20170363.

Bouckaert, R., J. Heled, D. Kühnert, T. Vaughan, C.-H. Wu, D. Xie, M. A. Suchard, A. Rambaut, and A. J. Drummond. 2014. BEAST 2: a software platform for Bayesian evolutionary analysis. Plos Comput Biol 10:e1003537.

Brely, L., F. Bosia, and N. M. Pugno. 2015. A hierarchical lattice spring model to simulate the mechanics of 2-D materials-based composites. Frontiers in Materials 2:51.

Cheng, D.-Q. and W. H. Piel. 2018. The origins of the Psechridae: Web-building lycosoid spiders. Mol Phylogenet Evol 125:213-219.

Coddington, J. A. 1986. The monophyletic origin of the orb web. Pp. 319-363 *in* W. A. Shear, ed. Spiders. Webs, Behavior, and Evolution. Stanford University Press, Stanford,CA.

Coddington, J. A. 2005. Phylogeny and classification of spiders. Pp. 18-24 *in* D. Ubick, P. Paquin, P. E. Cushing, and V. Roth, eds. Spiders of North America: an identification manual. . American Arachnological Society.

Coddington, J. A., I. Agnarsson, C. Hamilton, and J. E. J. P. P. Bond. 2018. Spiders did not repeatedly gain, but repeatedly lost, foraging webs. 6:e27341v27341.

Cook, R. D., D. S. Malkus, and M. E. Plesha. 2001. Concepts and applications of finite element analysis. John Wiley & Sons.

Cooper, N., G. H. Thomas, C. Venditti, A. Meade, and R. P. Freckleton. 2016. A cautionary note on the use of Ornstein Uhlenbeck models in macroevolutionary studies. Biol J Linn Soc 118:64–77.

Darriba, D., G. L. Taboada, R. Doallo, and D. Posada. 2012. jModelTest 2: more models, new heuristics and parallel computing. Nature methods 9:772.

Dawkins, R. 1982. The extended phenotype: The long reach of the gene. Oxford: Oxford University Press.

Donoghue, M. J. and D. D. Ackerly. 1996. Phylogenetic uncertainties and sensitivity analyses in comparative biology. Phil. Trans. R. Soc. Lond. B 351:1241-1249.

Drummond, A. J., S. Y. Ho, M. J. Phillips, and A. Rambaut. 2006. Relaxed phylogenetics and dating with confidence. PLoS biology 4:e88.

Duckworth, R. A. 2009. The role of behavior in evolution: a search for mechanism. Evolutionary ecology 23:513-531.

Eberhard, W. G. 1990. Function and phylogeny of spider webs. Annual review of Ecology and Systematics 21:341-372.

Eberhard, W. G. 2018a. Modular patterns in behavioural evolution: webs derived from orbs. Behaviour 155:531-566.

Eberhard, W. G., I. Agnarsson, and H. W. Levi. 2008. Web forms and the phylogeny of theridiid spiders (Araneae: Theridiidae): chaos from order. Systematics and biodiversity 6:415.

Eberhard, W. G. J. B. 2018b. Modular patterns in behavioural evolution: webs derived from orbs. 155:531-566.

Felsenstein, J. 1985. Phylogenies and the comparative method. The American Naturalist 125:1-15.

Fernández, R., G. Hormiga, and G. Giribet. 2014. Phylogenomic analysis of spiders reveals nonmonophyly of orb weavers. Curr Biol 24:1772-1777.

Fernández, R., R. J. Kallal, D. Dimitrov, J. A. Ballesteros, M. A. Arnedo, G. Giribet, and G. Hormiga. 2018. Phylogenomics, diversification dynamics, and comparative transcriptomics across the spider tree of life. Curr Biol 28:1489-1497.

Freckleton, R. P., P. H. Harvey, and M. Pagel. 2002. Phylogenetic analysis and comparative data: a test and review of evidence. The American Naturalist 160:712-726.

Garrison, N. L., J. Rodriguez, I. Agnarsson, J. A. Coddington, C. E. Griswold, C. A. Hamilton, M. Hedin, K. M. Kocot, J. M. Ledford, and J. E. Bond. 2016. Spider phylogenomics: untangling the Spider Tree of Life. PeerJ 4:e1719.

Grafen, A. 1989. The phylogenetic regression. Phil. Trans. R. Soc. Lond. B 326:119-157.

Hansell, M. H. 2005. Animal architecture. Oxford University Press, New York.

Ho, L. S. T. and C. Ané. 2014. Intrinsic inference difficulties for trait evolution with Ornstein-Uhlenbeck models. Methods in Ecology and Evolution 5:1133-1146.

Ingram, T. and D. L. Mahler. 2013. SURFACE: detecting convergent evolution from comparative data by fitting Ornstein-Uhlenbeck models with stepwise Akaike Information Criterion. Methods in Ecology and Evolution 4:416-425.

Kallal, R. J., R. Fernández, G. Giribet, and G. Hormiga. 2018. A phylotranscriptomic backbone of the orb-weaving spider family Araneidae (Arachnida, Araneae) supported by multiple methodological approaches. Mol Phylogenet Evol 126:129-140.

Katoh, K., J. Rozewicki, and K. D. Yamada. 2017. MAFFT online service: multiple sequence alignment, interactive sequence choice and visualization. Briefings in bioinformatics.

Kuntner, M., S. Kralj-Fišer, and M. Gregorič. 2010. Ladder webs in orb-web spiders: ontogenetic and evolutionary patterns in Nephilidae. Biol J Linn Soc 99:849-866.

Maddison, W. P., S. C. Evans, C. A. Hamilton, J. E. Bond, A. R. Lemmon, and E. M. Lemmon. 2017. A genome-wide phylogeny of jumping spiders (Araneae, Salticidae), using anchored hybrid enrichment. Zookeys:89.

Meijering, E., O. Dzyubachyk, and I. Smal. 2012. Methods for Cell and Particle Tracking. Methods in Enzymology 504:183-200.

Miller, M. A., W. Pfeiffer, and T. Schwartz. 2010. Creating the CIPRES Science Gateway for inference of large phylogenetic trees. Pp. 1-8. Gateway Computing Environments Workshop (GCE), 2010. Ieee.

Odling-Smee, F. J., H. Odling-Smee, K. N. Laland, M. W. Feldman, and F. Feldman. 2003. Niche construction: the neglected process in evolution. Princeton university press.

Opell, B. 1994. The ability of spider cribellar prey capture thread to hold insects with different surface features. Funct Ecol:145-150.

Opell, B. D. and H. S. Schwend. 2009. Adhesive efficiency of spider prey capture threads. Zoology 112:16-26.

Ord, T. J. and T. C. Summers. 2015. Repeated evolution and the impact of evolutionary history on adaptation. Bmc Evol Biol 15:137.

Ostoja-Starzewski, M. 2002. Lattice models in micromechanics. Applied Mechanics Reviews 55:35-60.

Ostrowski, A. M. 1973. The Newton-Raphson Method," Pure Appl. Math. Pp. 53-55 *in* A. M. Ostrowski, ed. Third Edition of Solution of Equations and Systems of Equations. Elsevier.

Paterno, G. B., C. Penone, and G. D. Werner. 2018. sensiPhy: An r-package for sensitivity analysis in phylogenetic comparative methods. Methods in Ecology and Evolution 9:1461-1467.

Pennell, M. W., J. M. Eastman, G. J. Slater, J. W. Brown, J. C. Uyeda, R. G. FitzJohn, M. E. Alfaro, and L. J. Harmon. 2014. geiger v2. 0: an expanded suite of methods for fitting macroevolutionary models to phylogenetic trees. Bioinformatics 30:2216-2218.

Piorkowski, D., S. Blamires, N. Doran, C. P. Liao, C. L. Wu, and I. M. Tso. 2018. Ontogenetic shift toward stronger, tougher silk of a web-building, cave-dwelling spider. J Zool 304:81-89.

Pugno, N. M. 2011. The theory of multiple peeling. Int J Fracture 171:185-193.

Pugno, N. M., S. W. Cranford, and M. J. Buehler. 2013. Synergetic material and structure optimization yields robust spider web anchorages. Small 9:2747-2756.

Revell, L. J. 2012. phytools: an R package for phylogenetic comparative biology (and other things). Methods in Ecology and Evolution 3:217-223.

Sahni, V., J. Harris, T. A. Blackledge, and A. Dhinojwala. 2012. Cobweb-weaving spiders produce different attachment discs for locomotion and prey capture. Nat Commun 3.

Salehani, M. K. and N. Irani. 2018. A coupled mixed-mode cohesive zone model: An extension to three-dimensional contact problems. arXiv preprint arXiv:1801.03430.

Schneider, C. A., W. S. Rasband, and K. W. Eliceiri. 2012. NIH Image to ImageJ: 25 years of image analysis. Nat methods 9:671-675.

Swanson, B., T. Blackledge, J. Beltrán, and C. Hayashi. 2006. Variation in the material properties of spider dragline silk across species. Applied Physics A 82:213-218.

Tung Ho, L. s. and C. Ané. 2014. A linear-time algorithm for Gaussian and non-Gaussian trait evolution models. Systematic biology 63:397-408.

Turner, J. S. and R. C. Soar. 2008. Beyond biomimicry: What termites can tell us about realizing the living building *in* I. Wallis, L. Bilan, M. Smith, and A. S. Kaz, eds. First International Conference on Industrialized, Intelligent Construction at Loughborough University.

Uyeda, J. C. and L. J. Harmon. 2014. A novel Bayesian method for inferring and interpreting the dynamics of adaptive landscapes from phylogenetic comparative data. Systematic biology 63:902-918.

Uyeda, J. C., R. Zenil-Ferguson, and M. W. Pennell. 2018. Rethinking phylogenetic comparative methods. Systematic Biology:syy031.

Wcislo, W. T. 1989. Behavioral environments and evolutionary change. Annual Review of Ecology and Systematics 20:137-169.

West-Eberhard, M. J. 1989. Phenotypic plasticity and the origins of diversity. Annual review of Ecology and Systematics 20:249-278.

Wheeler, W. C., J. A. Coddington, L. M. Crowley, D. Dimitrov, P. A. Goloboff, C. E. Griswold, G. Hormiga, L. Prendini, M. J. Ramírez, and P. Sierwald. 2017. The spider tree of life: phylogeny of Araneae based on target-gene analyses from an extensive taxon sampling. Cladistics 33:574-616.

Wolff, J. O. 2017. Structural effects of glue application in spiders – What can we learn from silk anchors? Pp. 63-80 *in* L. Xue, L. Heepe, and S. N. Gorb, eds. Bio-inspired structured adhesives. Springer Science+Business Media, Dordrecht.

Wolff, J. O., I. Grawe, M. Wirth, A. Karstedt, and S. N. Gorb. 2015. Spider's super-glue: thread anchors are composite adhesives with synergistic hierarchical organization. Soft Matter 11:2394-2403.

Wolff, J. O. and M. E. Herberstein. 2017. 3D-printing spiders: back-and-forth glue application yields silk anchorages with high pull-off resistance under varying loading situations. J R Soc Interface 14:20160783.

Wolff, J. O., A. van der Meijden, and M. E. Herberstein. 2017. Distinct spinning patterns gain differentiated loading tolerance of silk thread anchorages in spiders with different ecology. Proceedings of the Royal Society B: Biological Sciences 284:20171124.

York, R. A. and R. D. Fernald. 2017. The Repeated Evolution of Behavior. Frontiers in Ecology and Evolution 4:143.

Figures

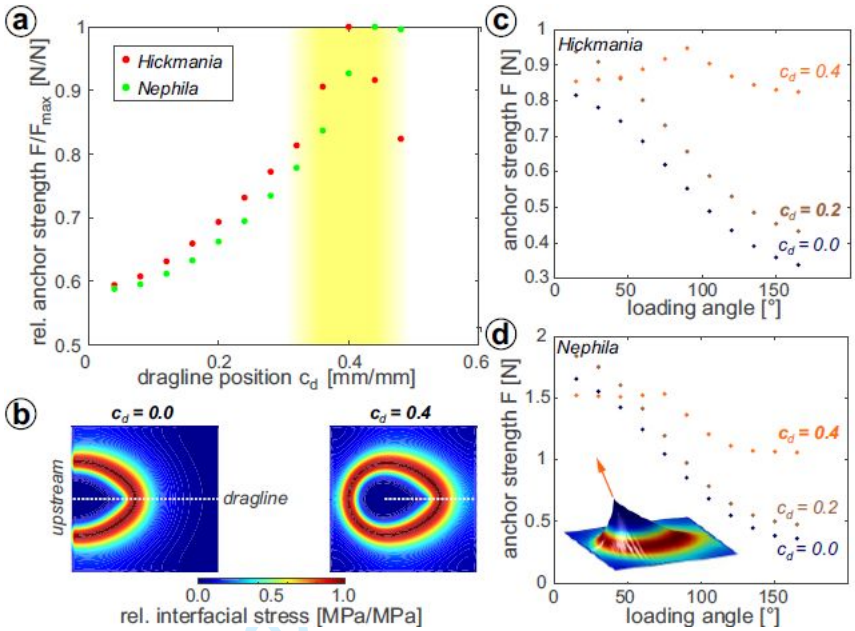

Fig. 1. Optimization of web anchor performance. ***(a)*** Simulated peak pull-off forces (anchor strength) vs. different dragline positions for silk properties of Tasmanian cave spiders (*Hickmania troglodytes*) and golden orb weavers (*Nephila plumipes*) under vertical load. The yellow shade indicates the estimated range of c_d (for a variety of silk properties), where anchor strength is maximized. ***(b)*** Exemplary maps of interfacial stress in the silk membrane (apical view) for an orb weaver silk anchor with $c_d = 0.0$ and $c_d = 0.4$ under vertical load. Warm colours indicate high stress. Anchors reach the peak pull-off force when the interfacial stress concentration around the peeling line reaches the membrane edge. ***(c)*** Simulated anchor strength for different dragline loading angles between 15° (± parallel to substrate along spinning direction) and 165° (± parallel to substrate against spinning direction, i.e. dragline flipped over) and three different values of c_d (different colours, bold font indicates the mean c_d naturally found in this species) for silk properties of Tasmanian cave spiders. ***(d)*** Same as in (c) for silk properties of golden orb weavers. Inset shows three-dimensional displacement map and stress distribution in an anchor with $c_d = 0.4$, pulled at an angle of 75° (top-side view).

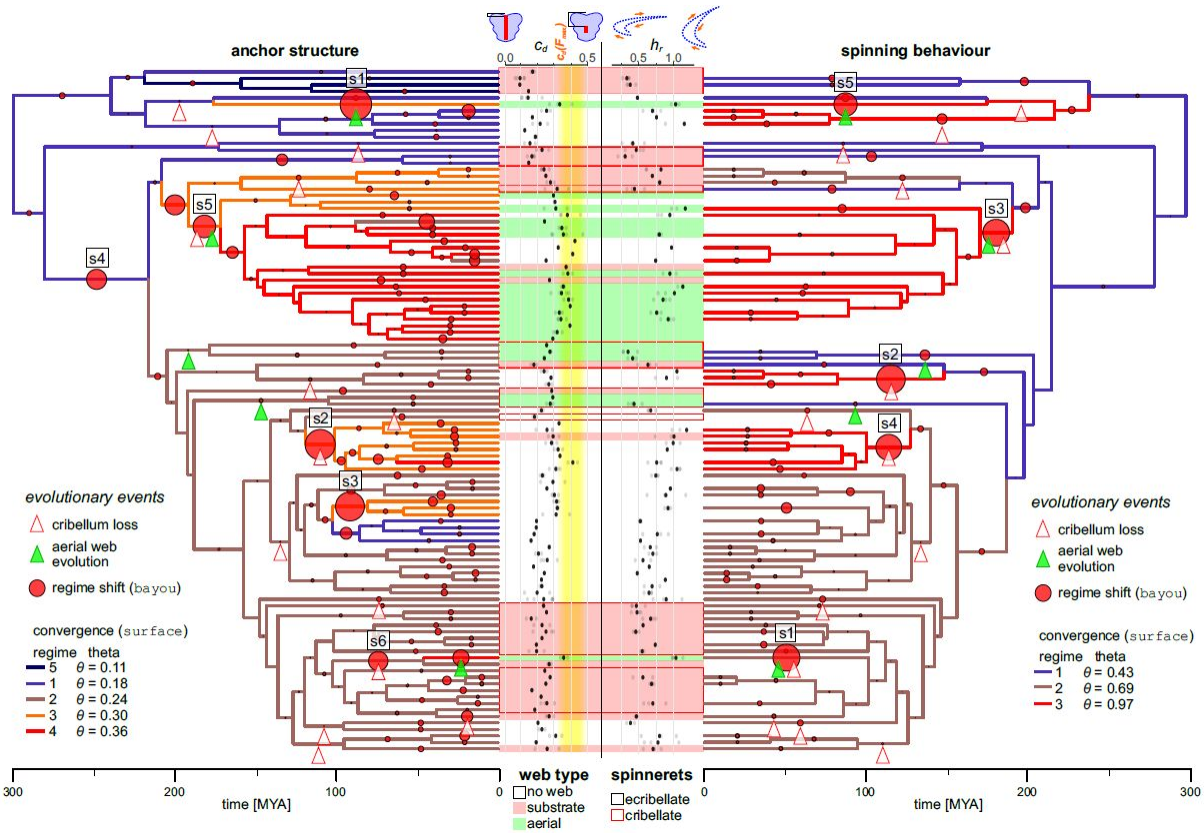

Fig. 2. Correlated evolution of web structure, behaviour and morphology. Shifts in the adaptive landscape of dragline placement c_d (left tree) and spinning choreography h_r (right tree). Branch colours denote convergent evolutionary regimes in the adaptive optimum θ as identified by *SURFACE*, with warmer colours indicating higher θs. The size of overlaid red pies indicates the posterior probability of a shift in θ in that branch, as found by *bayou*. Numbered shifts mark well supported shifts with $pp > 0.3$. White arrowheads with red outline indicate branches in which cribellum loss occurred, and green arrowheads indicate branches in which aerial web building has evolved (with a probability > 0.5). Dots at tips display c_d and h_r values measured in the extant species (grey dots represent means of individuals, black dot species means). The underlying shade indicates web building behaviour (white - no web, red - substrate web, green - aerial web) and the range of optimal anchor structure (yellow shade). Red boxes denote species with a cribellum. Schematics above symbolize anchors with a low and a high c_d (left; top view of anchor with membrane in blue and fused dragline in red) and spinning paths with a low and a high h_r (right; spinneret abducting to the right).

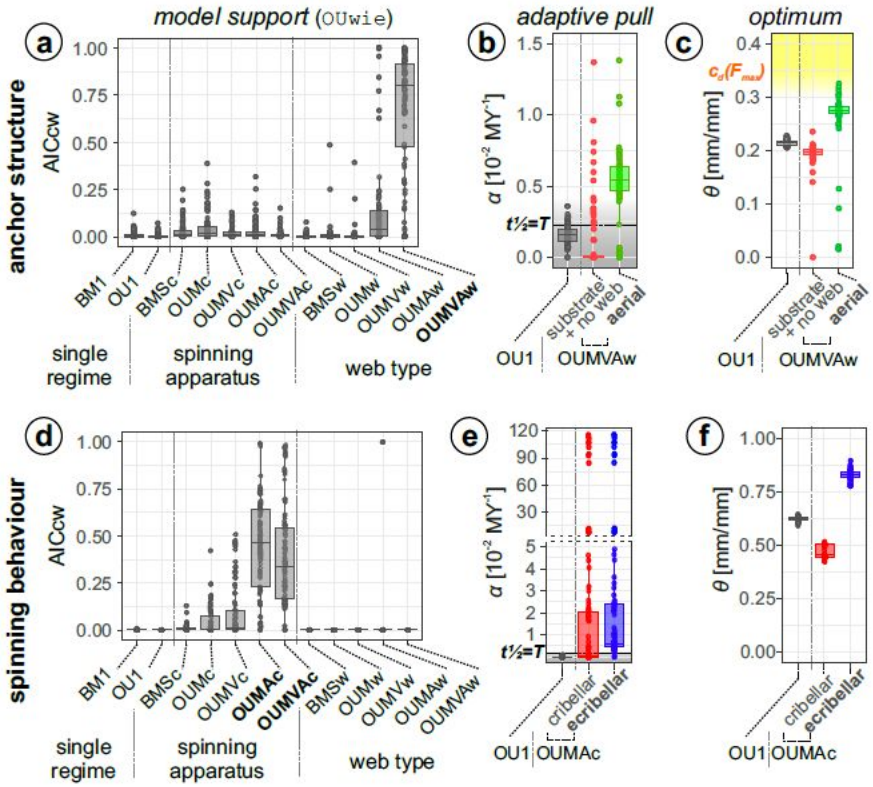

Fig. 3. Exceptional evolution of anchor structure in aerial web builders. ***(a)*** *AICc*-weight values for single- and two-regime evolutionary models of dragline placement c_d across 100 trees (best supporting model in bold font). A clear support for OUMAw and OUMVAw indicates that c_d evolved towards an elevated optimum and at a higher adaptive potential (and higher evolutionary rates) in aerial web builders. ***(b)*** Summary of adaptive potential α of c_d for single regime OU-models ('null'-model), and the two regimes of the best fitting OUw model across 100 trees (some extreme outliers not displayed). The black dotted line indicates an α for which the phylogenetic half-life $t½$ equals the total tree height T; below this threshold evolution becomes highly labile and BM-like (grey area). ***(c)*** Summary of the evolutionary optimum θ of c_d for single regime OU-models ('null'-model), and the two regimes of the best fitting OUw models across 100 trees. The yellow area indicates the theoretical physical optimum $c_d(F_{max})$. ***(d)*** Same as in (a) for spinning choreography h_r. A clear support for OUMAc and OUMVAc indicates that h_r evolved towards an elevated optimum and at a higher adaptive potential (and higher evolutionary rates) after cribellum loss. ***(e)*** Summary of adaptive potential α of h_r for single regime OU-models ('null'-model), and the two regimes of the best fitting OUc model across 100 trees. Same conventions as in (b). ***(f)*** Summary of the evolutionary optimum θ of h_r for single regime OU-models ('null'-model), and the two regimes of the best fitting OUc models across 100 trees. Same conventions as in (c).

673 **Electronic Supplemental Material (*ESM*)**
674
675 **S1.** Estimation of silk membrane stiffness.
676 **S2.** Comparing numerical model results of silk anchor efficiency with empirical data.
677 **S3.** Consensus tree.
678 **S4.** Ancestral character estimation
679 **S5.** Summary of SURFACE results.
680 **S6.** Summary of bayou results.
681 **S7.** Summary of PGLS results.
682 **S8.** Summary of geometric morphometrics results.
683 **S9.** Material list and sample sizes.
684 **S10.** Terminals mapping.
685 **S11.** Genbank identifiers.
686 **S12.** R code including data and tree files (zipped archive).